Chapter 2
Arclength Control-based Continuation for Autonomous Systems with Fast-Slow Dynamics

Alexandre Spits, Ghislain Raze, Marisa Saggio, Viktor Jirsa, and Gaëtan Kerschen

Abstract Bursting dynamics appear across a wide range of physical and biological systems, particularly in neuroscience, where they play a central role in modeling epilepsy. Epilepsy is characterized by abnormal, excessive or synchronous neuronal activity in the brain, marked by abrupt transitions from quiescent periods to seizures. Although EEG recordings help identify seizure patterns and affected brain regions, they often cannot predict precisely the onset, termination, or propagation of seizures. This poses a challenge for designing surgical interventions for the one-third of epilepsy patients who do not respond to medication. To deepen our understanding, phenomenological models based on nonlinear dynamics and bifurcation theory have been developed to classify seizure mechanisms by capturing fast-slow oscillations between ictal and interictal states.

Control-based continuation (CBC) techniques provide a powerful framework for experimentally exploring complex bifurcation diagrams of nonlinear systems. In this work, we present modifications to a recent extension of CBC, termed arclength control-based continuation (ACBC), for identifying fixed points and limit cycles in autonomous systems featuring fast-slow oscillations. While ACBC has been successfully applied in nonlinear vibration testing, where synchronization between the forcing and response frequencies simplifies signal analysis, autonomous systems present a unique challenge. Their self-sustained limit cycles have frequencies governed by internal dynamics which are not known a priori. To address this, we leverage angle-encoding to estimate the system's instantaneous phase and demonstrate its application within the context of seizure modeling.

Keywords Control-based continuation · Fast-slow bursters

Introduction

Nonlinear systems exhibit rich phenomena, including multistability and abrupt transitions between coexisting solutions under small parameter variations. To deal with such complex phenomena, bifurcation diagrams are used to trace the evolution of system responses and the points at which qualitative changes occur.

For decades, numerical continuation has been the standard tool for uncovering bifurcation diagrams [1–4]. It has advanced understanding across diverse engineering domains [5–8], yet its success relies on the availability of an accurate mathematical model. In many experimental settings, such models are either unavailable or too uncertain to capture the relevant dynamics. This limitation has motivated the development of experimental continuation methods [9], which combine non-invasive feedback control with continuation techniques to explore stable and unstable responses in a model-free manner.

The first experimental continuation method, known as control-based continuation (CBC) [10, 11], was conceived to extend numerical continuation principles to feedback-controlled experiments. In particular, this method leverages the Newton-Raphson algorithm and hence requires the determination of a Jacobian. Because estimating derivatives from experimental measurements is noise-sensitive and computationally expensive, derivative-free strategies were subsequently introduced.

Alexandre Spits · Ghislain Raze · Gaëtan Kerschen
Department of Aerospace & Mechanical Engineering, University of Liège, Liège, Belgium
e-mail: alexandre.spits@uliege.be; g.raze@uliege.be; g.kerschen@uliege.be

Marisa Saggio · Viktor Jirsa
Aix Marseille Univ, INSERM, INS, Inst Neurosci Syst, Marseille, France
e-mail: maria-luisa.SAGGIO@univ-amu.fr; viktor.jirsa@univ-amu.fr

© The Author(s), under exclusive license to River Publishers 2026

Kristin B. Zimmerman, PhD (eds.), *Nonlinear Structures & Systems, Vol. 1*, Conference Proceedings of the Society for Experimental Mechanics Series, https://doi.org/10.13052/rp-9788743814122

This evolution gave rise to two main approaches: simplified control-based continuation (SCBC) [12] and phase-locked loop (PLL) testing [13]. Both methods rely on parametrizing the system to unfold the nonlinear response curve and identify it by monotonically increasing the unfolding parameter. SCBC controls the fundamental harmonic of the response, whereas PLL adjusts the phase lag between the response and the excitation. When this parametrization fails to unfold the nonlinear response curve, these methods miss parts of the bifurcation diagram [9]. In contrast, state-of-the-art numerical continuation methods can traverse folds and recover the complete diagram. To bridge this gap, a new method, arclength control-based continuation (ACBC) [9, 14], was recently introduced. This approach adapts Crisfield's arclength principle [15] to SCBC, enabling navigation around fold bifurcations and uncovering the complete bifurcation diagram.

Experimental continuation techniques have been widely employed for forced nonlinear systems. SCBC has been used for frictional oscillators [16], geometrically nonlinear beams [17, 18], micro-electromechanical systems [19], and atomic force microscopy [20]. PLL testing has likewise been demonstrated on a variety of structures, including beams with geometric nonlinearities [21], beams with friction [22], and magnetic repulsion systems [23]. More recently, ACBC has been employed to experimentally explore electronic Duffing oscillators, clamped beams, and thin plates with geometric nonlinearities [9, 14]. More applications of these methods can be found in [9].

Unlike forced (non-autonomous) systems, autonomous systems have only rarely been explored with experimental continuation. In such systems, several behaviors may coexist, including stable or unstable equilibria and limit cycles, the latter being self-sustained oscillations that arise without external forcing. Whereas non-autonomous systems typically display synchronization between excitation and response frequencies, autonomous systems lack an external reference, and the frequency of a limit cycle emerges solely from the internal dynamics, which are generally unknown to the experimenter. This lack of a frequency reference introduces a phase indeterminacy, so a phase constraint must be imposed to uniquely define and track the limit cycle.

The first applications of control-based methods to obtain bifurcation diagrams for autonomous systems were demonstrated in aeroelastic systems [24, 25], cylindrical pipe flow simulations [26], synthetic biology [27], neuronal dynamics [28], and relaxation oscillations [29], using adapted versions of CBC. Distinct approaches are adopted depending on the type of bifurcation diagram to be identified: some target fixed point solutions, while others focus on limit cycles. In the former, the reference value is held constant until the controller converges, after which it is varied step by step. In the case of limit cycles, prediction and correction steps are carried out offline for each value of the bifurcation parameter. To enforce the phase constraint, these studies employed angle encoding [29]. Arclength control-based continuation has been applied to weakly nonlinear problems [30], where a PLL block is combined with ACBC to estimate the unknown phase.

The objective of this work is to investigate how arclength control-based continuation can be adapted to analyze autonomous systems with fast–slow dynamics. In this work, we place ourselves in the context of neuroscience, where such dynamics are particularly relevant. Neurons and neuronal populations naturally produce bursting, where episodes of fast oscillations alternate with quiescent phases. In epilepsy, such bursting reflects the alternation between interictal and ictal states, as observed in electroencephalography (EEG). Phenomenological models of seizure activity, such as those developed in [31, 32], describe these transitions using bifurcation theory and classify seizures according to the onset–offset bifurcations that generate them.

This work is structured as follows: we first introduce the fast–slow framework and the epileptic bursting model, then present the ACBC implementations for fixed-points and limit cycles, and finally demonstrate the method and discuss the resulting bifurcation diagrams.

Fast-slow Systems

Fast–slow systems are dynamical systems where different sets of variables evolve on widely separated timescales. They are often written in the general form

$$\frac{d\mathbf{x}}{dt} = f(\mathbf{x},\mathbf{z}), \qquad \frac{d\mathbf{z}}{dt} = c\,g(\mathbf{x},\mathbf{z}), \tag{1}$$

with $\mathbf{x} \in \mathbb{R}^m$ representing the fast variables, $\mathbf{z} \in \mathbb{R}^n$ the slow variables, and $0 < c \ll 1$ a small parameter controlling the timescale separation. Such systems can display complex dynamical features and are encountered in diverse areas.

To particularize the framework of fast–slow systems, we adopt the phenomenological model of epileptic bursting described in [31, 32]. This model is based on the unfolding of the degenerate Takens–Bogdanov singularity [33, 34] and represents seizure dynamics with two fast variables $\mathbf{x} = (x,y)$ and one slow variable $\mathbf{z} = z$. The fast subsystem is governed by

$$\begin{cases} \dot{x} = -y, \\ \dot{y} = x^3 - \mu_2(z)\,x - \mu_1(z) - y\big(\nu(z) + x + x^2\big), \end{cases} \tag{2}$$

where the linear and nonlinear terms shape the equilibria and oscillatory states of the fast subsystem. The coefficients $\mu_1(z)$, $\mu_2(z)$, and $\nu(z)$ vary with the slow variable z and shape how the bifurcations of the fast subsystem are organized.

Since z evolves on a much slower timescale than the fast variables, it can be regarded as fixed when analyzing the fast subsystem. In this fast-slow framework, the bifurcation diagram shows how the equilibria and limit cycles of the fast subsystem evolve with z. An example of such a bifurcation diagram is shown in Figure 1(a). The stable equilibria correspond to non-oscillatory states: the upper branch represents the interictal state, while the lower branch represents the active rest state considered ictal. The stable limit cycles, on the other hand, correspond to oscillatory ictal activity.

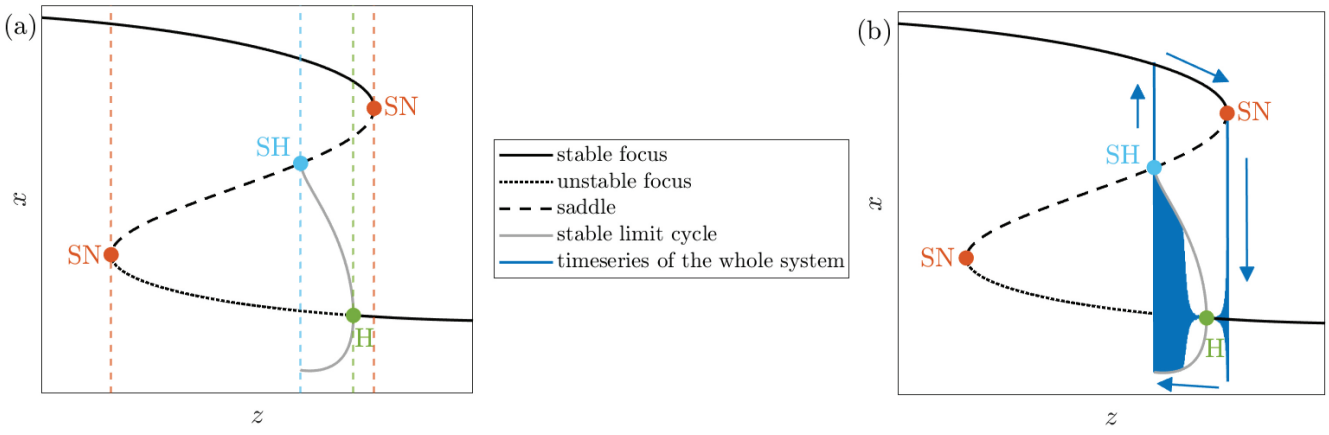


Fig. 1 Bifurcation diagram of the fast subsystem illustrating the mechanisms of seizure onset and offset. (a) Bifurcation diagram along the bursting path c10s [31], where Saddle-Node (SN), Hopf (H), and Saddle-Homoclinic (SH) bifurcations appear. (b) Example trajectory of the full system (blue) superimposed on the bifurcation diagram, showing the alternation between quiescent and oscillatory phases (interictal and ictal states) as the slow variable z drives the system through SN, H, and SH bifurcations

In the full model, the evolution of the slow variable z is given by

$$\dot{z} = -c\left(\sqrt{(x-x_s(z))^2+y^2}-d^*\right). \tag{3}$$

The dynamics of z are governed by the distance between the current state of the fast subsystem (x,y) and the silent state $(x_s(z),0)$. When the state lies within the threshold distance d^*, z changes only slowly, while during seizure-like oscillations the larger deviations of x gradually increase or decrease z. In this way, z captures a slow modulation of excitability and acts as a moving control parameter that continuously reshapes the dynamics of the fast subsystem.

As z drifts, it produces a hysteresis loop between rest and seizure, illustrated in Figure 1(b). Starting from a stable equilibrium (rest), z increases until a saddle–node bifurcation is crossed, after which the trajectory moves toward another attractor and z begins to decrease. A subsequent Hopf bifurcation gives rise to oscillations that mark seizure onset. These oscillations persist as z continues to evolve, until a saddle–homoclinic bifurcation is reached, where the limit cycle disappears and the system returns to rest, modelling seizure offset. This sequence generates bursting, alternating between quiescent and oscillatory activity.

This three-dimensional model is minimal yet sufficiently rich to capture essential features of epileptic bursting. In what follows, we apply control-based continuation methods, and in particular arclength control-based continuation (ACBC), to reconstruct the bifurcation diagram of the fast subsystem. The model is assumed unknown to the continuation procedure, which serves as a numerical validation and motivates further experimental applications.

Arclength control-based continuation for fast-slow systems

ACBC combines a feedback-controlled experiment with arclength continuation, a path-following technique. Each component serves a specific purpose, as detailed below. In autonomous systems, both equilibria and limit cycles can appear in the parameter space. An equilibrium is a time-invariant response where the system remains constant, while a limit cycle is a

time-periodic response corresponding to a self-sustained oscillation. Because of this intrinsic difference, the implementation of the method differs for the two cases, although the underlying principle remains the same.

Feedback control is required to stabilize unstable responses. In open-loop, sweeping the bifurcation parameter only reveals stable responses: near an unstable equilibrium or limit cycle, even small disturbances cause divergence and the response cannot be observed. At folds, the system undergoes sudden transitions between stable attractors, so that only a subset of stable branches is recovered. Upward and downward sweeps may reveal different stable solutions, yet others remain inaccessible.

Fixed-points identification

For fixed-point identification, the ACBC block diagram is shown in Figure 2.

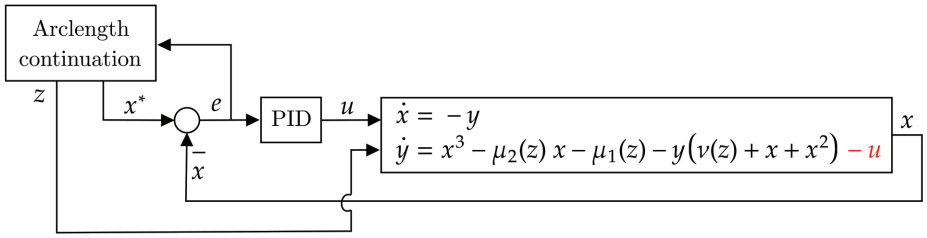


Fig. 2 ACBC block diagram for fixed-point identification in the autonomous system with fast-slow dynamics [31]. The control input u is applied to the fast dynamics

The system output $x(t)$ is compared with a reference $x^*(t)$, and the resulting error $e(t) = x^*(t) - x(t)$ drives the controller to adjust the system input $u(t)$. The controller's goal is to ensure that the response $x(t)$ converges toward the reference $x^*(t)$. With Proportional-Integral-Derivative (PID) control, the control action $u(t)$ is

$$u(t) = k_p\, e(t) + k_d \frac{d}{dt} e(t) + k_i \int_0^t e(t)\, dt, \tag{4}$$

where k_p, k_d, and k_i are the proportional, derivative, and integral gains. Both proportional and derivative control are required to stabilize the solutions, as each gain removes different bifurcations. Their combined effect unfolds the bifurcation diagram and enables access to unstable fixed points. A further analysis of how the control gains act on the system parameters $\mu_1(z)$, $\mu_2(z)$, and $\nu(z)$ can be found in the Appendix A, where local stability is examined through linearization of the controlled system with a Proportional-Derivative (PD) controller.

The control action is introduced into one of the equations governing the fast states, assuming it is experimentally feasible.

Stabilizing a response is distinct from ensuring its relevance. If the reference does not correspond to an open-loop response for a given bifurcation parameter, the closed-loop system cannot converge to the imposed reference, and the control action does not vanish. In this case, the resulting orbit does not correspond to any open-loop solution of the autonomous system, and the control is said to be invasive. Figure 3(a) shows with a colormap the regions of invasiveness in parameter space for different combinations of the reference value x^* and the bifurcation parameter z.

The continuation algorithm aims to determine the pairs (z, x^*) for which the control action vanishes, ensuring non-invasive responses. ACBC achieves this through a derivative-free adaptation of Crisfield's arclength continuation, where an integral control is introduced to perform continuation without derivatives. This integral control acts upfront of the PD controller previously described. In the (z, x^*) plane, the open-loop response is one-dimensional, as shown by the black curve in Figure 3(a). Starting from a known point (z_n, x_n^*) (white point), an ellipse (grey curve) is constructed and parametrized by an angle α:

$$(z(\alpha), x^*(\alpha)) = (z_n + \Delta z \cos\alpha,\ x_n^* + \Delta x^* \sin\alpha), \tag{5}$$

with Δz and Δx^* defining the semi-axes. The ellipse intersects the open-loop curve (black) at least twice (red and blue points), which corresponds to non-invasive solutions, while invasive ones arise along the sweep. The error associated with each point on the ellipse is shown in Figure 3(b). The integral control drives the system toward a non-invasive response by adjusting the arc angle α according to

$$\dot{\alpha}(t) = k_\alpha\, e(t), \tag{6}$$

where k_α is the integral gain. Its sign determines which of the intersections the control converges to, as illustrated in Figure 3(b). Once a new solution is reached, a new ellipse is centered at this point and the procedure is repeated to continue tracing the branch.

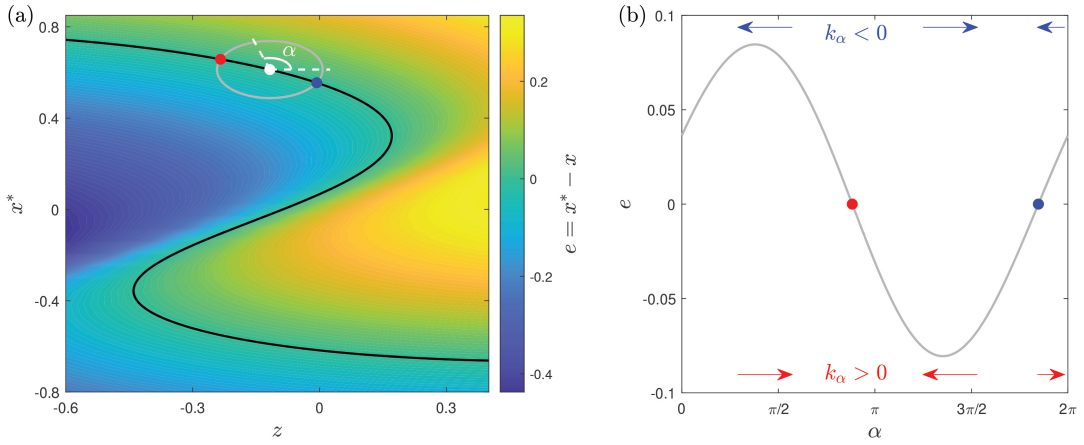


Fig. 3 (a) Colormap of the error between the imposed reference x^* and the converged response x, serving as an indicator of control invasiveness. The black curve represents the bifurcation diagram along the path c10s [31], corresponding to non-invasive control ($e = 0$). From a known point (white point), an ellipse (grey curve) is constructed to enable ACBC to identify two non-invasive solutions (red and blue points). (b) Evolution of the error $e = x^* - x$ along the ellipse parametrized by the angle α. The intersections of the ellipse with the bifurcation diagram are shown as in (a). The arrows indicate the direction of convergence of the integral control, depending on the sign of its gain k_α

The results obtained with ACBC for fixed-point identification are presented in the next section. The methodology is now extended to limit cycles.

Limit cycles identification

Limit cycles commonly originate from Hopf bifurcations and correspond to sustained oscillatory motion. They appear as closed trajectories in phase space. Figure 4(a-c) illustrates both their time evolution and their phase-plane representation in the fast–slow system previously introduced for modeling epilepsy. The frequency of a limit cycle depends on the system parameters and changes as these parameters are varied, as shown in Figure 4(e).

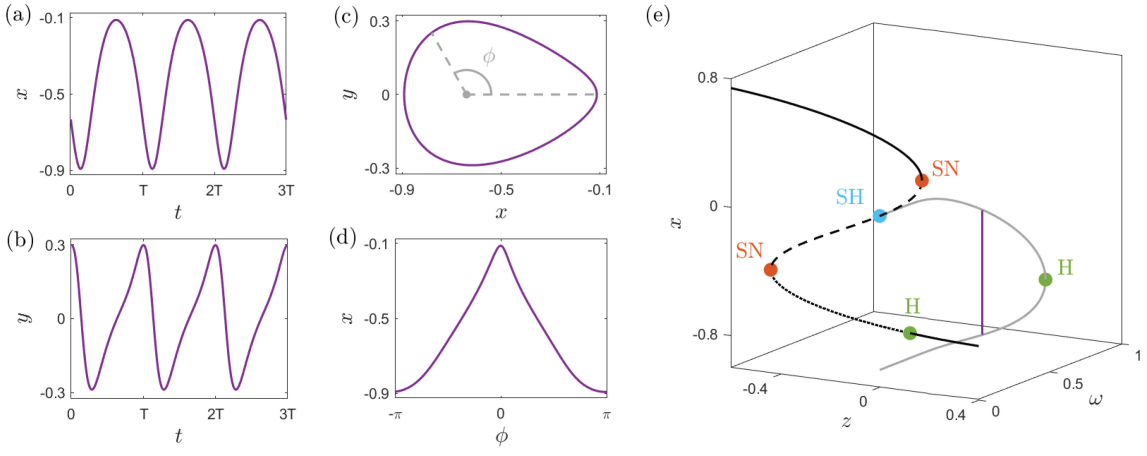


Fig. 4 (a–d) Representations of a given limit cycle: (a) time evolution of x, (b) time evolution of y, (c) phase portrait in the (x, y) plane, where the trajectory is parametrized by the angle ϕ (angle-encoding), (d) projection in the (x, ϕ) plane using this encoding. (e) Bifurcation diagram along the path c10s [31] in the space (z, ω, x). Equilibria (black) do not oscillate, while limit cycles (grey) do. The position of the limit cycle represented in (a-d) is illustrated in purple. Bifurcation points are labeled SN for Saddle-Node, H for Hopf, and SH for Saddle-Homoclinic

The absence of frequency information is a key difficulty in autonomous systems, where the frequency must be determined rather than imposed. In contrast, experimental continuation methods for non-autonomous systems, such as ACBC, prescribe the frequency as an input parameter, which typically leads to synchronization with the response. Adapting ACBC is therefore necessary in the autonomous case.

A convenient way to address this issue is to use an angle-encoding representation, where the motion along the limit cycle is described by a continuously evolving phase corresponding to a rotation along its closed trajectory. This is illustrated in Figure 4(c-d). This planar representation of the limit cycle is constructed from the measured response and another state of the system, such as $y = -\dot{x}$. The instantaneous phase ϕ is then defined as

$$\phi = \text{atan2}(y - \delta_y, x - \delta_x), \tag{7}$$

where (δ_x, δ_y) specifies the origin of the angle in the plane. For a unique angle to be assigned to every point, the chosen origin must lie inside the closed trajectory. A scaling factor may also be introduced to improve the distribution of the angle. Although another variable could be used instead of a system state, it must still provide a unique mapping between the angle and the position on the limit cycle.

This representation removes the need to impose or measure the frequency, as the phase is obtained from the system dynamics via the corresponding angle in the state space. The approach was introduced in the context of control-based continuation in [29].

Using the angle-encoding procedure, ACBC can be formulated for limit cycles. As in the case of fixed-point identification, it is structured as a combination of several blocks, as illustrated in Figure 5. Stabilization is still achieved through feedback of the response $x(t)$, which is compared with the reference $x^*(t)$ and processed by a PD controller (see Equation (4)), defining the control action applied to the autonomous system.

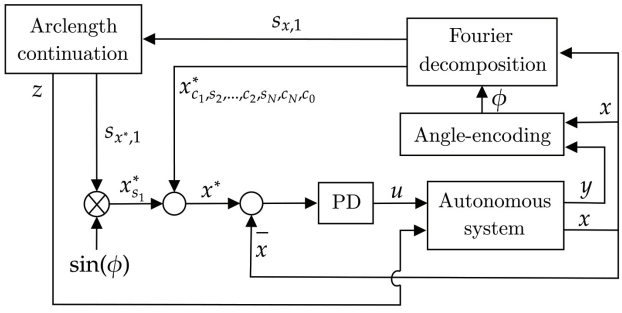


Fig. 5 ACBC Block diagram for limit cycle identification in an autonomous system with fast-slow dynamics. The control input u is applied to the fast dynamics

The difference lies in how the reference signal is constructed: oscillatory responses require additional blocks compared to the fixed-point case. The system considered in Equation (2) is nonlinear, and nonlinear systems generate harmonics in their response. All signals can therefore be decomposed into harmonic components. Using a truncated Fourier decomposition with N harmonics, any periodic signal $v(t)$ at steady state can be expressed as

$$\begin{aligned} v(t) &= \sum_{n=0}^{N} c_{v,n}\cos(n\phi) + s_{v,n}\sin(n\phi) \\ &= \sum_{n=0}^{N} v_{c_n}(t) + v_{s_n}(t) \end{aligned} \tag{8}$$

where $c_{v,n}$ and $s_{v,n}$ are the Fourier coefficients of the n-th harmonic. The goal is to construct a reference that cancels every harmonic present in the response, ensuring zero control action and thus stabilizing a non-invasive solution. To achieve this, the phase ϕ must be consistently defined between the response and the reference, a constraint enforced by angle encoding.

In practice, the Fourier decomposition is performed in real time using adaptive filters [9, 14]. These filters estimate the Fourier coefficients $c_{v,n}$ and $s_{v,n}$ by minimizing the error between the measured response and its approximation through the least mean square (LMS) algorithm. This adaptive approach avoids the need for offline procedures such as Picard iterations or B-spline fitting.

Not all Fourier coefficients are handled in the same way. Arclength continuation acts on one of the fundamental coefficients of the reference, for instance $s_{x^*,1}$, and searches in the parameter space $(z, s_{x^*,1})$ for the right couple that satisfies

the condition $s_{x^*,1} = s_{x,1}$. The remaining harmonic coefficients of the response are directly copied into the reference. This prevents additional control action from higher-order components.

The arclength continuation works in the same way as previously, except that the working plane has changed. This is illustrated in Figure 6(a). As previoulsy, an integral controller is used to drive the search along the ellipse, defined by the law,

$$\dot{\alpha} = k_\alpha (s_{x^*,1} - s_{x,1}). \tag{9}$$

Along the search, non-invasive solutions are encountered, but this controller allows to identify intersections with the uncontrolled limit cycle branch (see Figure 6(b)). The results obtained with ACBC for limit cycle identification are presented in the next section.

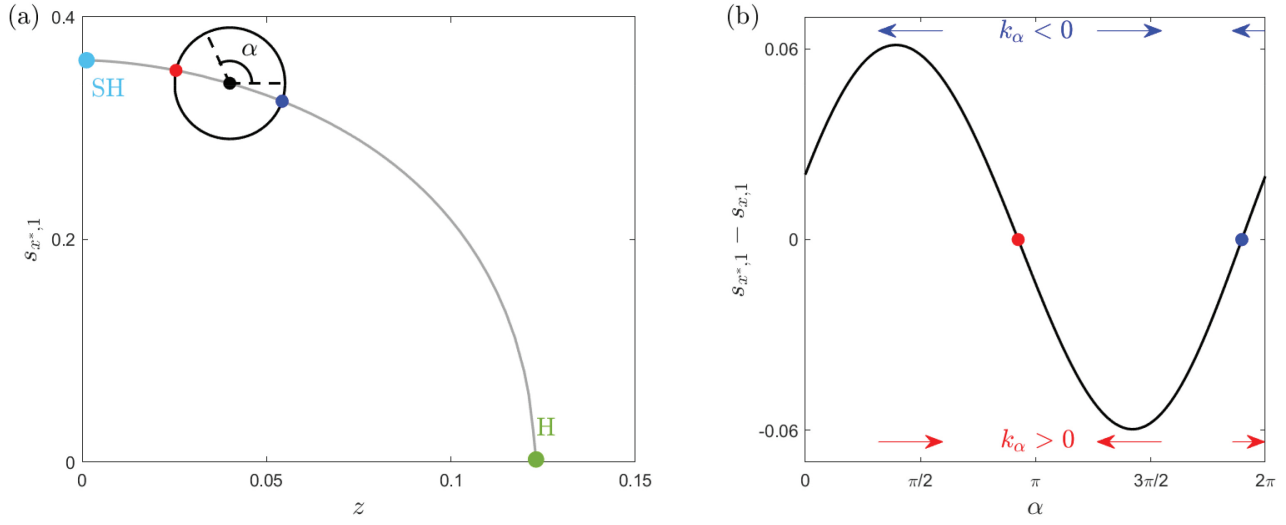


Fig. 6 (a) Working plane of the ACBC used for limit cycle identification. The grey curve represents the non-invasive solutions. From a known point (black point), an ellipse (black curve) is constructed to enable ACBC to identify two non-invasive solutions (red and blue points). (b) Evolution of the error between the sine Fourier coefficient of the first harmonic for the reference $s_{x^*,1}$ and the response $s_{x,1}$ along the ellipse parametrized by the angle α. The points where non-invasive control is achieved are shown as in (a). The arrows indicate the direction of convergence of the integral control, depending on the sign of its gain k_α

Results

Bifurcation diagrams of autonomous systems associated with bursting dynamics comprise both fixed points and limit cycles, including stable and unstable branches. To capture the complete set of solutions, two different implementations of ACBC were employed. Figure 7 illustrates two such diagrams for the bursting paths c10s and c16s [31], providing a comparison between ACBC and MatCont [4]. ACBC was also used to uncover further bifurcation diagrams corresponding to additional bursting paths from [31], which are presented in the Appendix B.

An excellent agreement is obtained between the numerical responses. ACBC successfully tracks both stable and unstable branches and smoothly continues through folds in fixed-point as well as limit-cycle solutions. In Figure 7(b), an unstable limit cycle branch emerges after the fold bifurcation and terminates at the Hopf bifurcation. Accurate tuning of the control gains is required to capture the entire branch. Stabilization near the Hopf bifurcation is particularly challenging, since the control tends to converge toward the stable fixed point branch. According to [29], the choice of the origin affects the performance of the controller. Here the objective is not to discuss performance but to demonstrate that combining distinct blocks can realize ACBC for limit cycles. For limit cycle identification with ACBC, it was essential to keep the center of the angle-encoding within the closed trajectory in the phase plane. Future work could explore adaptive adjustment of the center based on the previously identified limit cycle.

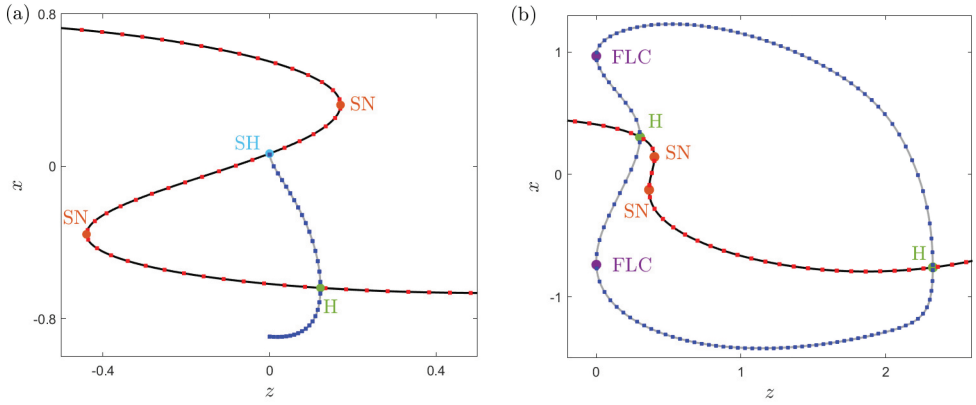


Fig. 7 Bifurcation diagrams along the bursting trajectories: (a) c10s and (b) c16b. Limit cycles from MatCont [4] (grey lines) and ACBC (blue dots) are displayed together with fixed points from MatCont (black lines) and ACBC (red dots). Stability is not indicated. Bifurcation points are marked as SN for Saddle-Node, H for Hopf, and FLC for Fold Limit Cycle

Conclusion

This work extends arclength control-based continuation (ACBC) to autonomous systems with fast–slow dynamics. By combining angle encoding with adaptive filters, the method captures both equilibria and limit cycles, including unstable branches. Numerical results on bursting paths c10s and c16s of the generalized Epileptor model confirm the ability of ACBC to reconstruct complete bifurcation diagrams. Because the approach is model-free, it can be directly applied in experiments, offering a powerful tool to probe complex dynamics such as those underlying epilepsy.

Acknowledgments Alexandre Spits and Ghislain Raze are a research fellow and a postdoctoral researcher, respectively, of the Fonds de la Recherche Scientifique - FNRS, which is gratefully acknowledged. Marisa Saggio has received funding from the European Union's Horizon Europe Programme under the Specific Grant Agreement No. 101147319 (EBRAINS 2.0 Project).

Appendix A

To better understand how control gains affect the dynamics of the system, particularly their influence on the effective unfolding parameters $\mu_1(z)$, $\mu_2(z)$, and $\nu(z)$ of the uncontrolled system, it is useful to analyze the local stability around equilibrium points (x_P, y_P). Stabilization of any response near equilibrium can be approached by linearizing the controlled system. For nonlinear systems, the local stability of a hyperbolic equilibrium is entirely determined by the linearized dynamics in its vicinity. Here, we consider the case of a proportional plus derivative (PD) controller applied to the system, resulting in the following closed-loop equations:

$$\begin{cases} \dot{x} = -y, \\ \dot{y} = x^3 - \mu_2(z)x - \mu_1(z) - y(\nu(z) + x + x^2) - k_p(x^* - x) + k_d(y^* - y). \end{cases} \tag{10}$$

To linearize the system around a given fixed point (x_P, y_P), a perturbation $(\delta x, \delta y)$ of the equilibrium can be considered, i.e.,

$$x = x_P + \delta x, \text{ and } y = y_P + \delta y. \tag{11}$$

Note that $y_P = 0$ since $\dot{x} = -y$ and we are considering fixed points ($\dot{x} = \dot{y} = 0$).

Introducing the perturbation from Eq. (11) into the closed-loop equations Eq. 10, we have:

$$\begin{cases} \dfrac{d}{dt}(x_P + \delta x) = -\delta y, \\ \dfrac{d}{dt}(\delta y) = x_P^3 + 3x_P^2\,\delta x + 3x_P\,\delta x^2 + \delta x^3 - \mu_2(z)\,x_P - \mu_2(z)\,\delta x - \mu_1(z) \\ -\delta y\,\nu(z) - \delta y\,x_P - \delta y\,\delta x - \delta y\,x_P^2 - 2\,\delta y\,\delta x\,x_P - \delta y\,\delta x^2 - k_p\,x^* + k_p\,x_P \\ +k_p\,\delta x + k_d\,y^* - k_d\,\delta y. \end{cases} \tag{12}$$

Considering only first-order terms in δx and δy and removing constant terms with respect to the perturbations, we obtain:

$$\begin{cases} \delta\dot{x} = -\delta y, \\ \delta\dot{y} = 3x_P^2\,\delta x - \mu_2(z)\,\delta x - \delta y\,\nu(z) - \delta y x_P - \delta y x_P^2 + k_p\,\delta x - k_d\,\delta y. \end{cases} \tag{13}$$

Only terms proportional to δx, δy, and their time derivatives remain. Rewriting the nonlinear dynamics in general form:

$$\begin{cases} \dot{x} &= f(x,y), \\ \dot{y} &= g(x,y). \end{cases} \tag{14}$$

the Jacobian matrix is defined by linearizing the system into its state-space form:

$$\delta\dot{\mathbf{v}} = \mathbf{J}\,\delta\mathbf{v}, \tag{15}$$

or:

$$\begin{bmatrix} \delta\dot{x} \\ \delta\dot{y} \end{bmatrix} = \begin{bmatrix} \dfrac{\partial f}{\partial x} & \dfrac{\partial f}{\partial y} \\ \dfrac{\partial g}{\partial x} & \dfrac{\partial g}{\partial y} \end{bmatrix}_{(x_P,y_P)} \begin{bmatrix} \delta x \\ \delta y \end{bmatrix} \tag{16}$$

Using Eq. 13 to identify the Jacobian terms, the Jacobian matrix writes:

$$\mathbf{J} = \begin{bmatrix} 0 & -1 \\ 3x_P^2 - \mu_2(z) + k_p & -(\nu(z) + x_P + x_P^2 + k_d) \end{bmatrix} \tag{17}$$

The trivial solution of this linear system is asymptotically stable if and only if all the roots of the characteristic polynomial $\det(\mathbf{J} - \lambda\mathbf{I}) = 0$ have negative real parts. For a second-order system, this is equivalent to requiring that all the coefficients a_i in the polynomial $a_2\lambda^2 + a_1\lambda + a_0 = 0$ are strictly positive. In our case, the characteristic equation becomes:

$$\lambda^2 + (\nu(z) + x_P + x_P^2 + k_d)\lambda + 3x_P^2 - \mu_2(z) + k_p = 0. \tag{18}$$

Hence, the stability conditions are:

$$\nu(z) + x_P + x_P^2 + k_d > 0 \quad \text{and} \quad 3x_P^2 - \mu_2(z) + k_p > 0, \tag{19}$$

which can be rewritten as:

$$k_d > -(\nu(z) + x_P + x_P^2) \quad \text{and} \quad k_p > -3x_P^2 + \mu_2(z). \tag{20}$$

These conditions are directly influenced by the value of the bifurcation parameter z. While the physical meaning of the individual coefficients may not be immediately clear, they offer important guidance on how the choice of control gains affects the stability boundaries of the system across different dynamical regimes. Note that the linearized stability condition applies only locally.

With suitable values of the control gains k_p and k_d satisfying the stability conditions obtained through linearization, the controller alters the bifurcation diagram so that unstable branches and bifurcations are no longer present.

Appendix B

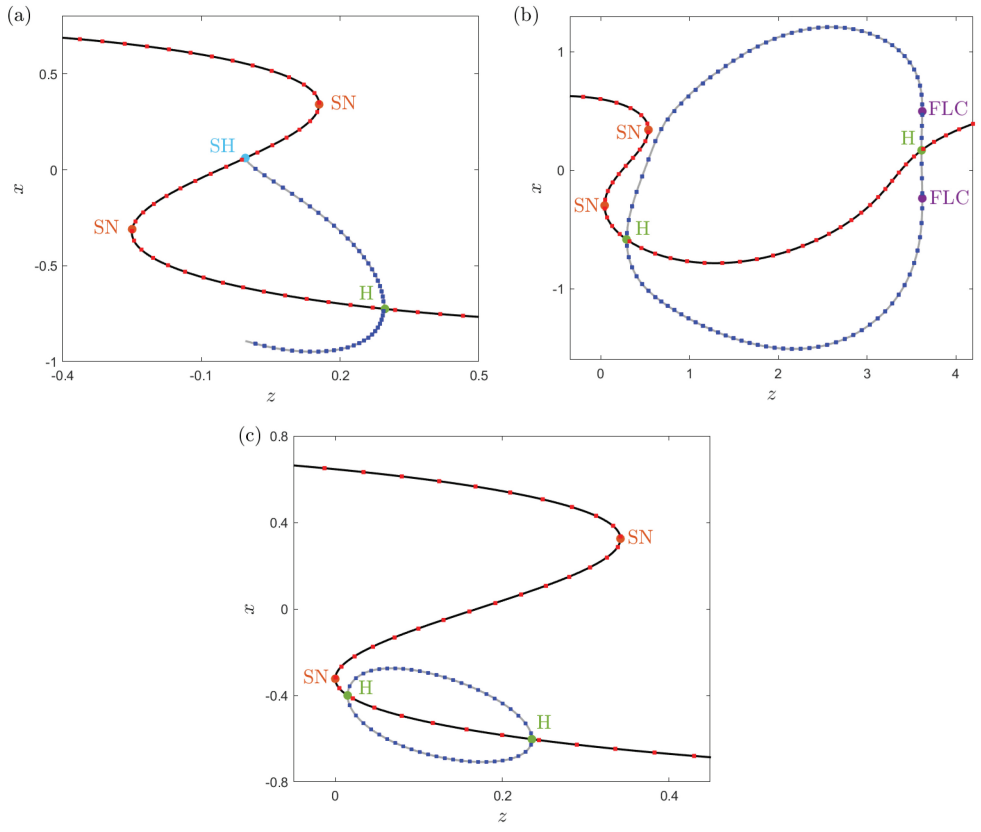


Fig. 8 Bifurcation diagrams along the bursting trajectories: (a) c2s, (b) c3s, and (c) c11s. Limit cycles from MatCont [4] (grey lines) and ACBC (blue dots) are displayed together with fixed points from MatCont (black lines) and ACBC (red dots). Stability is not indicated. Bifurcation points are marked as SN for Saddle-Node, H for Hopf, and FLC for Fold Limit Cycle

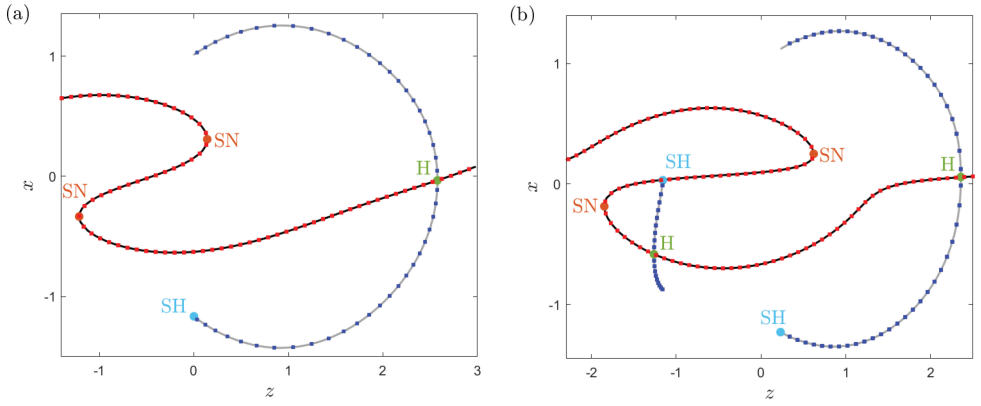


Fig. 9 Bifurcation diagrams along the bursting trajectories: (a) c2b and (b) c14b. Limit cycles from MatCont [4] (grey lines) and ACBC (blue dots) are displayed together with fixed points from MatCont (black lines) and ACBC (red dots). Stability is not indicated. Bifurcation points are marked as SN for Saddle-Node, H for Hopf, and FLC for Fold Limit Cycle

References

1. Keller, H.B. "Numerical solution of bifurcation and nonlinear eigenvalue problems". In Rabinowitz, P.H., editor, *Applications of Bifurcation Theory*, pages 359–384. Academic Press, New York (1977)
2. Allgower, E.L. and Georg, K. *Introduction to Numerical Continuation Methods*. SIAM, Philadelphia (2003)
3. Seydel, R. *Practical Bifurcation and Stability Analysis: From Equilibrium to Chaos*, volume 5 of *Interdisciplinary Applied Mathematics*. Springer-Verlag, Berlin, Heidelberg, New York, London, Paris, Tokyo, Hong Kong, 2 edition (1994)
4. Govaerts, W.J. *Numerical Methods for Bifurcations of Dynamical Equilibria*, volume 4 of *Monographs on Mathematical Modeling and Computation*. SIAM, Philadelphia (2000)
5. Knowles, J.A.C., Krauskopf, B., and Lowenberg, M.H. "Numerical continuation applied to landing gear mechanism analysis". *Journal of Aircraft*, 48(4):1254–1262 (2011)
6. Detroux, T., Renson, L., Masset, L., and Kerschen, G. "The harmonic balance method for bifurcation analysis of large-scale nonlinear mechanical systems". *Comput. Methods Appl. Mech. Eng.*, 296:18–38 (2015)
7. Dankowicz, H. and Schilder, F. "An extended continuation problem for bifurcation analysis in the presence of constraints". *Journal of Computational and Nonlinear Dynamics*, 6(3):031003 (2010)
8. Fréour, V., Guillot, L., Masuda, H., Usa, S., Tominaga, E., Tohgi, Y., Vergez, C., and Cochelin, B. "Numerical continuation of a physical model of brass instruments: Application to trumpet comparisons". *J. Acoust. Soc. Am.*, 148(2):748–758 (2020)
9. Raze, G., Abeloos, G., and Kerschen, G. "Experimental continuation in nonlinear dynamics: Recent advances and future challenges". *Nonlinear Dyn.*, 113(6):4949–4997 (2025)
10. Sieber, J., Gonzalez-Buelga, A., Neild, S.A., Wagg, D.J., and Krauskopf, B. "Experimental continuation of periodic orbits through a fold". *Phys. Rev. Lett.*, 100(24):244101 (2008)
11. Sieber, J. and Krauskopf, B. "Control based bifurcation analysis for experiments". *Nonlinear Dynamics*, 51(3):365–377 (2008)
12. Barton, D.A.W. and Sieber, J. "Systematic experimental exploration of bifurcations with noninvasive control". *Phys. Rev. E*, 87(5):052916 (2013)
13. Peter, S. and Leine, R.I. "Excitation power quantities in phase resonance testing of nonlinear systems with phase-locked-loop excitation". *Mech. Syst. Signal Process.*, 96:139–158 (2017)
14. Abeloos, G. *Control-based methods for the identification of nonlinear structures*. PhD thesis, University of Liège (2022)
15. Crisfield, M.A. "A fast incremental/iterative solution procedure that handles "snap-through"". *Comput. Struct.*, 13(1–3):55–62 (1981)
16. Kleyman, G., Paehr, M., and Tatzko, S. "Application of control-based-continuation for characterization of dynamic systems with stiffness and friction nonlinearities". *Mechanics Research Communications*, 106:103520 (2020)
17. Hayashi, S., Gutschmidt, S., Murray, R., et al. "Experimental bifurcation analysis of a clamped beam with designed mechanical nonlinearity". *Nonlinear Dynamics*, 112:15701–15717 (2024)
18. Abeloos, G., Renson, L., Collette, C., et al. "Stepped and swept control-based continuation using adaptive filtering". *Nonlinear Dynamics*, 104:3793–3808 (2021)
19. Hayashi, S., Cameron, C., Gutschmidt, S., et al. "Experimentally characterising the dynamical landscape of an active mems cantilever". *Research Square* (2025) Preprint, Version 1.
20. Böttcher, L., Wallner, H., Kruse, N., Just, W., Barke, I., Starke, J., and Speller, S. "Exposing hidden periodic orbits in scanning force microscopy". *Communications Physics*, 8(1):57 (2025)
21. Scheel, M., Peter, S., Leine, R., and Krack, M. "A phase resonance approach for modal testing of structures with nonlinear dissipation". *Journal of Sound and Vibration*, 435:56–73 (2018)
22. Scheel, M., Weigele, T., and Krack, M. "Challenging an experimental nonlinear modal analysis method with a new strongly friction-damped structure". *Journal of Sound and Vibration*, 485:115580 (2020)
23. Scheel, M., Kleyman, G., Tatar, A., Brake, M., Peter, S., Noël, J.P., Allen, M., and Krack, M. "Experimental assessment of polynomial nonlinear state-space and nonlinear-mode models for near-resonant vibrations". *Mechanical Systems and Signal Processing*, 143:106796 (2020)
24. Tartaruga, I., Barton, D.A.W., Rezgui, D., and Neild, S.A. "Experimental bifurcation analysis of a wing profile". In *Proceedings of the International Forum on Aeroelasticity and Structural Dynamics (IFASD)*, Savannah, Georgia, USA (2019)
25. Lee, K.H., Barton, D.A.W., and Renson, L. "Model identification of a fluttering aerofoil using control-based continuation and normal form analysis". In *Proceedings of ISMA2020 and USD2020*, pages 261–268, Leuven, Belgium (2020)
26. Willis, A.P., Duguet, Y., Omel'chenko, O.E., and Wolfrum, M. "Surfing the edge: finding nonlinear solutions using feedback control". *Journal of Fluid Mechanics*, 831:579–591 (2017)
27. de Cesare, I., Salzano, D., di Bernardo, M., Renson, L., and Marucci, L. "Control-based continuation: A new approach to prototype synthetic gene networks". *ACS Synthetic Biology*, 11(7):2300–2313 (2022)
28. Amakhin, D., Chizhov, A., Girier, G., Desroches, M., Sieber, J., and Rodrigues, S. "Observing hidden neuronal states in experiments". *arXiv preprint* (2025) arXiv:2308.15477 [q-bio.NC].
29. Blyth, M., Tsaneva-Atanasova, K., Marucci, L., and Renson, L. "Numerical methods for control-based continuation of relaxation oscillations". *Nonlinear Dynamics*, 111(78):7975–7992 (2023)
30. Gourc, E., Caron, R., Silva, F., Vergez, C., and Cochelin, B. "Theoretical analysis of a derivative free control based continuation algorithm with path following capability for autonomous systems". HAL preprint, hal-05042729 (2025)
31. Saggio, M.L., Spiegler, A., Bernard, C., and Jirsa, V.K. "Fast–slow bursters in the unfolding of a high codimension singularity and the ultra-slow transitions of classes". *The Journal of Mathematical Neuroscience*, 7(1):7 (2017)
32. Saggio, M.L. and Jirsa, V. "Bifurcations and bursting in the epileptor". *PLoS Computational Biology*, 20(3):e1011903 (2024)
33. Dumortier, F., Roussarie, R., and Sotomayor, J. "Generic 3-parameter families of vector fields on the plane, unfolding a singularity with nilpotent linear part. the cusp case of codimension 3". *Ergodic Theory and Dynamical Systems*, 7(3):375–413 (1987)
34. Dumortier, F., Roussarie, R., Sotomayor, J., and Żołądek, H. *Bifurcations of Planar Vector Fields: Nilpotent Singularities and Abelian Integrals*, volume 1480 of *Lecture Notes in Mathematics*. Springer, Berlin (1991)